International Journal of Modern Physics B
Vol. 38, No. 18 (2024) 2450234 (19 pages)

DOI: 10.1142/S0217979224502345

Hydro-magneto-thermal aspects of ternary composite nanomaterial over arbitrarily inclined thin needle influenced by linear and nonlinear slips

S. S. Samantaray*, A. Misra*, S. Shaw†, M. Azam‡, Ali J. Chamkha§ and M. K. Nayak¶,‖

*Department of Mathematics,
Centurion University of Technology and Management,
Paralakhemundi, Gajapati 761211, Odisha, India

†Department of Mathematics and Statistical Sciences,
Botswana International University of Science and Technology,
Private Bag 16, Palapye, Botswana

‡School of Mathematics and Statistics, Yulin University,
Yulin 719000, P. R China

§Faculty of Engineering, Kuwait College of Science and Technology,
Doha 35004, Kuwait

¶Department of Mechanical Engineering, ITER,
Siksha 'O' Anusandhan Deemed to be University,
Bhubaneswar 751030, India
‖mkn2122@gmail.com

Received 14 January 2023
Revised 17 February 2023
Accepted 5 March 2023
Published 18 July 2023

Because of accelerated demands of advanced technologies like power station, chemical production and microelectronics, it necessitates the need of novel type of fluids with more heat transfer capability. Due to synergistic effect, ternary composite nanofluids (TCNFs) ensure better thermophysical and Rheology properties thereby acting as better suitable heat transfer fluid in wire coating, metal spinning, aerodynamics, medicine and engineering industries, etc. In view of such relevance, flow and heat transfer aspects of TCNF MWCNT + Al_2O_3 + TiO_2 + water induced by linear and nonlinear slips over arbitrarily inclined moving thin needle are investigated in this study. Thompson and Troian nonlinear slip model is modified by developing it in polar coordinates. Quadratic thermal radiation phenomenon is adopted. Fourth-order Runge–Kutta method is used to obtain requisite numerical solution. Major outcomes indicate that fluid velocity of TCNF whittles down with amplification of magnetic parameter due to the flow induced by either linear or nonlinear slips. Lower value of Reynolds number favoring linear slip leads to effective intensification of nondimensional temperature

‖Corresponding author.

distributions. Surface viscous drag and heat transfer rate get ameliorated with growth in size of thin needle under the influence of both linear and nonlinear slips.

Keywords: MHD; ternary composite nanofluid; modified Thompson and Troian slip; quadratic thermal radiation.

PACS numbers: 44.40 +a, 65.80 +n, 68.65 –k.

1. Introduction

Amelioration of heat transportation by nanofluids leads to wide range of applications in photonics, heat exchangers, electronics, chillers, boiler and energy associated industries.[1] These nanofluids comprise of base fluid and nanometer-sized particles (formed of metals, carbides, carbon nanotubes, metals or oxides).[2,3] To understand how diverse nanofluid compositions can improve conduction qualities, many researchers have studied the subject.[4–8] Later, binary composite nanofluids and their flow and thermal behavior subject to several surfaces under different constraints were examined by many researchers. For instance, Akinshilo and Ali[9] studied double diffusive magnetohydrodynamic squeezing flow of nanofluid between two parallel disks with slip and temperature jump boundary conditions. Nayak *et al.*[10] discussed 3D radiative convective flow of ZnO-SAE50nano-lubricant in presence of varying magnetic field and heterogeneous reactions. They observed that the enhanced strength of magnetic field controls the flow of ZnO-SAE50nano-lubricant. Akinshilo[11] investigated the nanofluid conveying porous medium through nonparallel plates using the Akbari–Ganji method. Zidan *et al.*[12] studied the thermal management and natural convection flow of nanoencapsulated phase change material (NEPCM)–water suspension in a reverse T-shaped porous cavity enshrining two hot baffles, Sobamowo and Akinshilo[13] analyzed the squeezing flow of nanofluid between two parallel plates under the influence of magnetic field. They observed that rise in magnetic parameter leads to decelerated motion of nanofluid. Nayak *et al.*[14] investigated the efficacy of diverse structures of wavy baffles on heat transfer amplification of double-diffusive natural convection inside a C-shaped enclosure filled with hybrid nanofluid. Akinshilo and llegbusi[15] investigated Lorentz force effect on steady nanofluid flow and heat transfer through parallel plates.

A theoretical model for the heat conduction of binary composite nanofluids has been developed by Chougule and Sahu.[16] Further, Akinshilo *et al.*[17] studied thermal and entropy generation analysis of hybrid nanofluid flow through stretchable rotating system with heat source/sink. They found that increasing volume of nanoparticles concentration ameliorates entropy generation. The effect of nanoparticle volume concentration depicts an increase in Bejan's number. Wang *et al.*[18] assessed the effective thermal conductivity of fluid and nanoparticles mixed. In addition, Selvakumar and Suresh[19] investigated how cooling electronic components with a hybrid $CuO–Al_2O_3$/water nanofluid would affect the environment. Huang *et al.*[20] investigated superiority of binary composite nanofluid over simple nanofluids in

terms of high heat transfer rate and low pressure drop. Nayak *et al.*[21] examined entropy optimized assisting and opposing nonlinear radiative flow of hybrid nanofluid. The increase in temperature ratio parameter leads to the enhancement of fluid temperature as observed in their study. Further, Nayak *et al.*[22] carried out a numerical investigation of Numerical computation for entropy generation in Darcy–Forchheimer transport of hybrid nanofluids with Cattaneo–Christov double diffusion.

Ternary composite nanofluids (TCNFs) were established to achieve more effective outcomes in terms of the augmentation of heat transfer, despite the fact that nanofluids/binary composite nanofluids have diversified engineering applications in fluid flows because of their improved thermal properties. Compared to straightforward nanofluids, they exhibit thermophysical characteristics that are substantially better. Simultaneous improvement of both thermophysical and heat transfer properties together could be attained in TCNFs. Because of such outstanding properties, TCNFs are used in energy transport and several thermal transmission applications such as solar collectors, heat pipes, heat exchangers, minichannel heat sink and others. Recent years have visualized development of very few experimental models of TCNFs as well as studies exploiting them. For instance, Dezfulizadeh *et al.*[23] examined an experimental study on dynamic viscosity and thermal conductivity of water–Cu–SiO_2–MWCNT TCNFs. Xuan *et al.*[24] analyzed on sensitivity and thermoeconomic aspects of TCNFs. Sahoo[25] discussed thermohydraulic properties of radiator using TCNFs. Quero and Rosenkranz[26] explored the performance of binary and ternary composite MXene/nanocellulose hydrogels and aerogels. Boroomandpour *et al.*[27] investigated thermal conductivity of a TCNF with MWCNTs TiO_2–ZnO/water EG (80:20). Kashyap *et al.*[28] explored the regenerative evaporative cooler efficiency by using TCNFs. The device yields the highest coefficient of performance, exergy efficiency and sustainability index; however, surface modification leads to higher running cost and equivalent CO_2 emission. Sarangi *et al.*[29] analyzed rotational flow and thermal behavior of ternary hybrid nanomaterials at small and high Prandtl numbers. Their numerical results conveyed that prominent decelerated flow of ternary hybrid nanofluid (THNF) is attained due to amplification of rotation parameter in Darcy–Forchheimer medium subject to both low Pr ($\mathrm{Pr} = 0.01$) and high Pr ($\mathrm{Pr} = 10,000$) than unary nanofluid (UNF). Axial velocity peters out by 11.76% (at low Pr ($\mathrm{Pr} = 0.01$)) and 12.5% (at high Pr ($\mathrm{Pr} = 10,000$)) for THNF while it whittles down by 21.42% (at low Pr) and 20% (high Pr) for UNF subject to fluid (UNF/THNF) flows in Darcy medium ($F_r = 0$) and non-Darcy medium ($F_r = 3$). In addition, heat transfer rate from the rotating surface emaciates significantly by 119% for THNF at $\mathrm{Br} = 1.5$, $\mathrm{Bi} = 1$ from low Pr ($\mathrm{Pr} = 0.01$) to high Pr ($\mathrm{Pr} = 10,000$). Further, Sarangi *et al.*[30] investigated hydrothermal behavior and irreversibility analysis of Bödewadt flow of radiative and dissipative ternary composite nanomaterial due to a stretched rotating disk. The ternary composite/hybrid nanomaterial is a mixture of water as base fluid and Al_2O_3, graphene and MWCNT as nanoparticles. The numerical solution is obtained

by using bvp4c method through MATLAB. The most important physical conclusion of the present investigation is that introduction of TCNF to the Bödewadt flow over a stretched rotating disk gives rise to controlled motion subject to slip condition reduces surface viscous drag effectively and ameliorates heat transfer rate thereby imparting significant cooling compared to binary hybrid nanofluid and mono nanofluid.

The boundary layer flow over thin needle is applied in wind velocity measurement, wire coating, aerodynamics, etc. As far as boundary layer flow over thin needle is concerned, works such as boundary layer flow,[31] boundary layer flow induced by a parallel-free stream,[32] assisting and opposing flows,[33] nonlinear thermal radiation effect,[34] heat generation and nonlinear radiation effects,[35] buoyancy driven convective MHD flow,[36] and EMHD flow of non-Newtonian nanofluids[37] were carried on effectively.

Taking intensive literature survey and analyzing the works there, it is visualized that the effect of linear and nonlinear slips on flow and heat transfer of TCNF over arbitrarily inclined (horizontal-inclined and vertical-inclined) thin needle subject to quadratic thermal radiation is yet to be investigated. The objective of this study is to investigate the flow and heat transfer of radiative and dissipative TCNF over arbitrarily inclined thin needle influenced by linear and nonlinear slips. The novelty of this study includes the following aspects:

- Linear and nonlinear slip effects featured in Modified Thompson and Troian slip model are newly considered.
- Quadratic thermal radiation model is newly introduced in flow over thin needle.
- TCNF flow is newly implemented over thin needle.

2. Mathematical Description and Equations of the Physical Model

In the present problem, we consider a steady, laminar boundary layer flow of TCNF over an arbitrarily inclined (horizontal-inclined and vertical-inclined) thin needle moving with a constant velocity U_w. Assume that water as base fluid is dispersed with ternary nanoparticles such as MWCNT, Al_2O_3, TiO_2 in order to ameliorate thermal conductivity of water so as to make it as best coolant. A uniform magnetic field of strength B_0 is assumed to be applied normal to the stretching surface of thin needle. The magnetic Reynolds number is considered to be small and therefore the induced magnetic field and electric field are neglected.

The following assumptions are made for the present problem:

- There is no pressure gradient along the thin needle.
- Let the radius of thin needle be $r = R(x)$, where r and x represent radial and axial coordinates, respectively.
- Modified Troian and Thomson slip model is considered.
- Quadratic thermal radiation phenomenon is implemented.

- Magnetohydrodynamic flow pattern is adopted.
- Viscous dissipation as well as Ohmic heating is taken into account.
- Convective boundary condition is introduced.

Figures 1 and 2 depict the flow geometry and the related coordinate system. Under the above assumptions, the boundary layer equations framed are

Continuity equation

$$\frac{\partial}{\partial x}(ru) + \frac{\partial}{\partial r}(rv) = 0. \tag{1}$$

Momentum equation for horizontal-inclined needle

$$u\frac{\partial u}{\partial x} + v\frac{\partial u}{\partial r} = \upsilon_{\mathrm{TCNF}}\left(\frac{\partial^2 u}{\partial r^2} + \frac{1}{r}\frac{\partial u}{\partial r}\right) + g\beta_{\mathrm{TCNF}}(T - T_\infty)\sin\Omega - \frac{\sigma_{\mathrm{TCNF}}B_0^2 u}{\rho_{\mathrm{TCNF}}}. \tag{2}$$

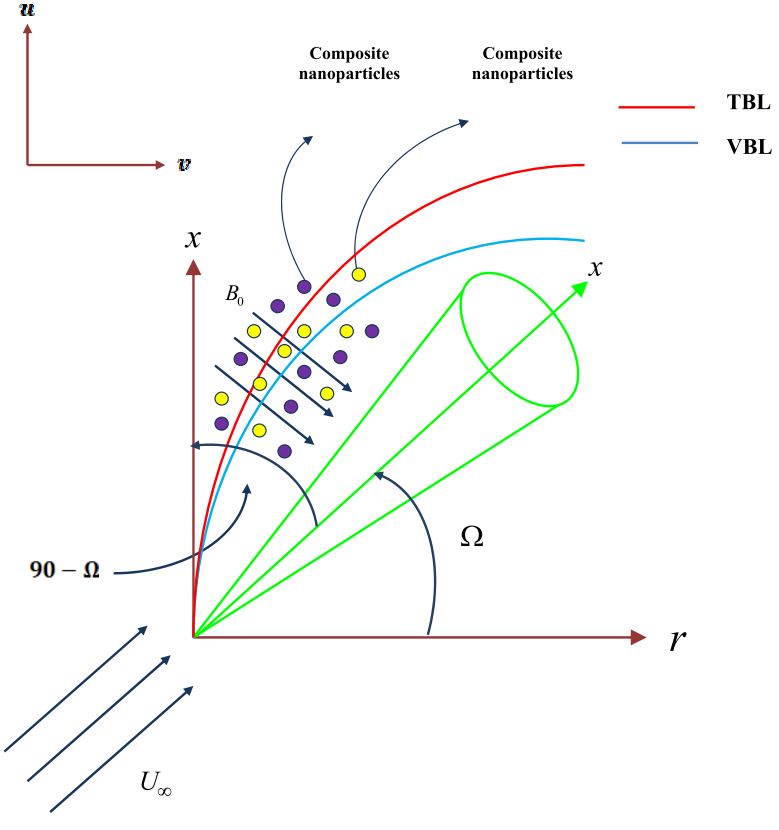

Fig. 1. (Color online) Flow geometry of horizontally-inclined needle.

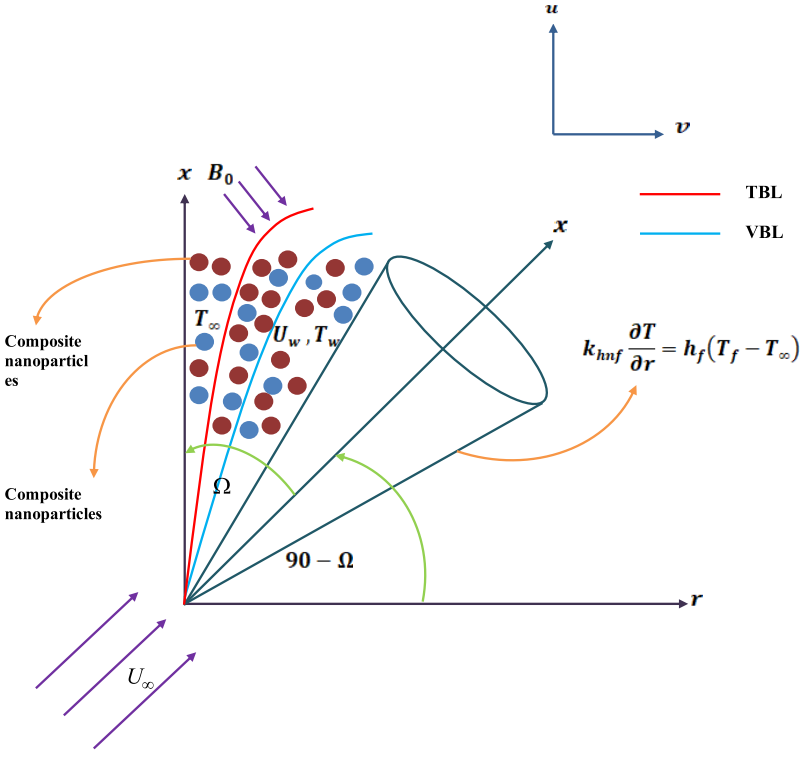

Fig. 2. (Color online) Flow geometry of vertically-inclined needle.

Momentum equation for vertical-inclined needle

$$u\frac{\partial u}{\partial x}+v\frac{\partial u}{\partial r}=\upsilon_{\mathrm{TCNF}}\left(\frac{\partial^2 u}{\partial r^2}+\frac{1}{r}\frac{\partial u}{\partial r}\right)+g\beta_{\mathrm{TCNF}}(T-T_\infty)\sin(90^\circ-\Omega)-\frac{\sigma_{\mathrm{TCNF}}B_0^2 u}{\rho_{\mathrm{TCNF}}}. \tag{3}$$

Energy equation

$$u\frac{\partial T}{\partial x}+v\frac{\partial T}{\partial r}=\alpha_{\mathrm{TCNF}}\frac{1}{r}\frac{\partial}{\partial r}\left(r\frac{\partial T}{\partial r}\right)+\frac{48\sigma^* T_\infty^2}{3k^*(\rho c_p)_{\mathrm{TCNF}}}\times\left\{\frac{1}{r}\left(T\frac{\partial T}{\partial r}\right)+\left(\frac{\partial T}{\partial r}\right)^2+T\frac{\partial^2 T}{\partial r^2}\right\}-\frac{32\sigma^* T_\infty^3}{3k^*(\rho c_p)_{\mathrm{TCNF}}}\times\left\{\frac{1}{r}\frac{\partial T}{\partial r}+\frac{\partial^2 T}{\partial r^2}\right\}+\frac{\mu_{\mathrm{TCNF}}}{(\rho c_p)_{\mathrm{TCNF}}}\left(\frac{\partial u}{\partial r}\right)^2+\frac{\sigma_{\mathrm{TCNF}}B_0^2 u^2}{(\rho c_p)_{\mathrm{TCNF}}}. \tag{4}$$

Boundary conditions

$$\left.\begin{aligned} u = U_w + \underbrace{\frac{\gamma^*\left\{r\frac{d}{dr}\left(\frac{u}{r}\right)\right\}}{\left[1-\delta^* r\frac{d}{dr}\left(\frac{u}{r}\right)\right]^{\frac{1}{2}}}}_{\text{Modified } T \text{ hom pson and Troian slip}}, \qquad v = 0, \\ -k_{\mathrm{TCNF}}\frac{\partial T}{\partial r} = h_f(T_f - T) \quad \text{at } r = R, \\ u = U_\infty, \quad T \to T_\infty \quad \text{as } r \to \infty \end{aligned}\right\}. \tag{5}$$

Here, u and v, respectively, are the axial and radial components of velocity, μ_{TCNF}, υ_{TCNF}, ρ_{TCNF}, β_{TCNF}, σ_{TCNF}, $(\rho C_p)_{\mathrm{TCNF}}$, α_{TCNF}, k_{TCNF} are, respectively, dynamic viscosity, kinematic viscosity, density, thermal expansion coefficient, electrical conductivity, specific heat capacity, thermal diffusivity, thermal conductivity of TCNF, B_0 is uniform magnetic field strength, (T, T_∞) are temperature of TCNF within boundary layer and ambient, g is gravitational acceleration, Ω is the tilting angle, σ^* is Stefan–Boltzmann constant, k^* is mean absorption coefficient, γ^* is slip length (m) and δ^* is the inverse of the critical shear rate (s).

Physical, thermal and electrical properties ternary composite nanofluid

The thermophysical properties of TCNF are

The density of TCNF is[25,28]

$$\rho_{\mathrm{TCNF}} = \phi_1\rho_1 + \phi_2\rho_2 + \phi_3\rho_3 + (1 - \phi_1 - \phi_2 - \phi_3)\rho_f, \tag{6}$$

where ρ_1, ρ_2, ρ_3 are the densities, ϕ_1, ϕ_2, ϕ_3 are the volume fractions of first, second and third nanoparticles, respectively, ρ_f is the density of base fluid.

The specific heat capacity of TCNF[25,28]

$$(\rho C_p)_{\mathrm{THNF}} = \phi_1(\rho C_p)_1 + \phi_2(\rho C_p)_2 + \phi_3(\rho C_p)_3 + (1 - \phi_1 - \phi_2 - \phi_3)(\rho C_p)_f, \tag{7}$$

where $(\rho C_p)_1, (\rho C_p)_2, (\rho C_p)_3$ are specific heat capacities of first, second and third nanoparticles, respectively, and $(\rho C_p)_f$ is the specific heat capacity of base fluid.

The dynamic viscosity of TCNF is[25,28]

$$\mu_{\mathrm{TCNF}} = \frac{(\phi_1\mu_{\mathrm{nf},1} + \phi_2\mu_{\mathrm{nf},2} + \phi_3\mu_{\mathrm{nf},3})}{\phi}, \tag{8}$$

where $\mu_{\mathrm{nf},1}, \mu_{\mathrm{nf},2}, \mu_{\mathrm{nf},3}$ are dynamic viscosities of first, second and third nanoparticles, respectively.

The thermal conductivity of TCNF is[25,28]

$$k_{\mathrm{TCNF}} = \frac{\left(\phi_1 k_{\mathrm{nf},1} + \phi_2 k_{\mathrm{nf},2} + \phi_3 k_{\mathrm{nf},3}\right)}{\phi}, \tag{9}$$

where $k_{\mathrm{nf},1}, k_{\mathrm{nf},2}, k_{\mathrm{nf},3}$ are thermal conductivities of first, second and third nanoparticles, respectively. Here, $\phi = \phi_1 + \phi_2 + \phi_3$ is the total volume fraction.

For ith nanoparticle suspension (of given shape), we have

$$\mu_{\mathrm{nf},i} = \mu_f(1 + B_i\phi + C_i\phi^2), \tag{10}$$

$$\frac{k_{\mathrm{nf},i}}{k_f} = \frac{k_{p,i} + (m_i - 1)k_f + (m_i - 1)\phi(k_{p,i} - k_f)}{k_{p,i} + (m_i - 1)k_f - \phi(k_{p,i} - k_f)}, \tag{11}$$

where B and C are viscosity enhancement coefficients.

Similarity transforms

$$\left.\begin{aligned} u &= 2Uf'(\eta), \qquad v = -\frac{\upsilon_f}{r} f + \eta \frac{\upsilon_f}{r} f'(\eta), \\ \theta(\eta) &= \frac{T - T_\infty}{T_w - T_\infty}, \quad \eta = \frac{Ur^2}{\upsilon_f x} \end{aligned}\right\}, \tag{12}$$

where U the sum of is U_w and U_∞. By setting $\eta = A$ (refers to the wall of needle) in Eq. (12), $R(x) = \left(\frac{Avx}{U}\right)^{1/2}$ is the surface shape of axisymmetric body.

Nondimensional governing equations

Using Eqs. (6)–(12) in Eqs. (2)–(5), we have

$$\left(\frac{\mu_{\mathrm{TCNF}}}{\mu_f}\right)\left(\frac{\rho_f}{\rho_{\mathrm{TCNF}}}\right)(f'' + 2\eta f''') + ff'' + f''(1 + 2\mathrm{We}f'') + \frac{1}{4}\lambda_1\left(\frac{\beta_{\mathrm{TCNF}}}{\beta_f}\right)\theta \sin\Omega - \frac{1}{2}\left(\frac{\sigma_{\mathrm{hnf}}}{\sigma_f}\right)\left(\frac{\rho_f}{\rho_{\mathrm{TCNF}}}\right)Mf' = 0, \tag{13}$$

$$\left(\frac{\mu_{\mathrm{TCNF}}}{\mu_f}\right)\left(\frac{\rho_f}{\rho_{\mathrm{TCNF}}}\right)(f'' + 2\eta f''') + ff'' + f''(1 + 2\mathrm{We}f'') + \frac{1}{4}\lambda_1\left(\frac{\beta_{\mathrm{TCNF}}}{\beta_f}\right)\theta \sin(90^0 - \Omega) - \frac{1}{2}\left(\frac{\sigma_{\mathrm{hnf}}}{\sigma_f}\right)\left(\frac{\rho_f}{\rho_{\mathrm{TCNF}}}\right)Mf' = 0, \tag{14}$$

Table 1. Thermophysical properties of base fluid (water) and nanoparticles (MWCNT, Al_2O_3, TiO_2) at 300 K.[38]

Physical properties	Water	MWCNT	Al_2O_3	TiO_2
Specific heat capacity (J/kg K)	4179	410	765	686.2
Thermal conductivity (W/m K)	0.613	3007.4	40	8.9538
Density (kg m^{-3})	997.1	2100	3970	4250
Electrical conductivity (S m^{-1})	0.05	0.5×10^4	10^{-12}	0.1×10^{-12}
Thermal expansion coefficient ($\beta \times 10^{-5} K^{-1}$)	21	1.6	0.85	0.9
Shape	Spherical	Cylindrical	Spherical	Spherical

Table 2. Parameters for describing shape and properties of nanoparticles.[38]

Shape of nanoparticles	B	C	m
Platelets	37.1	612.6	5.7
Cylindrical	13.5	704.4	4.9
Spherical	2.5	6.2	3

$$\frac{k_{\text{hnf}}}{k_f}\left(\frac{\mu_{\text{TCNF}}}{\mu_f}\right)\left(\frac{(\rho C_p)_f}{(\rho C_p)_{\text{TCNF}}})(\theta' + 2\eta\theta''\right) + \Pr f\theta'$$
$$+ R\left(\frac{(\rho C_p)_f}{(\rho C_p)_{\text{TCNF}}}\right)[8(1+\theta\theta_D)(\theta' + 2\eta\theta'') + 16\eta\theta_D(\theta')^2 - 4(\theta' + 2\eta\theta'')]$$
$$+ 4\left(\frac{(\rho C_p)_f}{(\rho C_p)_{\text{TCNF}}}\right)\text{ReBr}(f'')^2 + \frac{\sigma_{\text{hnf}}}{\sigma_f}\left(\frac{(\rho C_p)_f}{(\rho C_p)_{\text{TCNF}}}\right)M\ \text{Br}(f')^2 = 0. \tag{15}$$

Nondimensional boundary conditions

$$\left.\begin{aligned} &f'(A) = \frac{1}{2}\varepsilon + \frac{\gamma\left[2f''(A) - \frac{1}{A}f'(A)\right]}{\left[1 - \delta\left\{f''(A) - \frac{2}{A}f'(A)\right\}\right]^{\frac{1}{2}}}, \quad f(A) = Af'(A), \\ &\frac{k_{\text{TCNF}}}{k_f}\theta'(A) = -\frac{1}{2}\text{Bi}[1 - \theta(A)], \\ &f'(\infty) = \frac{1}{2}(1-\varepsilon), \quad \theta(\infty) \to 0 \end{aligned}\right\}. \tag{16}$$

Nondimensional parameters

$$\left.\begin{aligned} &M = \frac{\sigma_f B_0^2 x}{U\rho_f}, \quad \lambda = \frac{g\beta_f(T_f - T_\infty)x}{U^2}, \quad \theta_D = \frac{T_f - T_\infty}{T_\infty}, \\ &R = \frac{4\sigma^* T_\infty^3}{3k^* k_f}, \quad \Pr = \frac{\upsilon_f}{\alpha_f}, \quad E_c = \frac{U^2}{(c_p)_f(T_f - T_\infty)}, \quad \text{Br} = \Pr E_c, \\ &\gamma = \gamma^*\frac{Ur}{\upsilon_f x}, \quad \delta = \frac{\delta^* U^2 r}{\upsilon_f x}, \quad \text{Re} = \frac{Ur}{\upsilon_f}, \quad \varepsilon = \frac{U_w}{U}, \quad \text{Bi} = \frac{h_f}{k_f\left(\frac{Ur}{\upsilon_f x}\right)} \end{aligned}\right\}. \tag{17}$$

Here, $M, \lambda, \theta_D, R, \Pr, E_c, \text{Br}, \text{Re}, \gamma, \delta, \varepsilon, \text{Bi}$, respectively, represent magnetic parameter, mixed convection parameter, temperature difference parameter, quadratic thermal radiation parameter, Prandtl, Eckert, Brinkman and Reynolds numbers, velocity slip parameter, modified inverse of critical shear rate, velocity ratio parameter, Biot number.

Parameters of importance

The skin friction and Nusselt number are, respectively,

$$\text{Re}_x^{\frac{1}{2}} C_f = 8\frac{\mu_{\text{TCNF}}}{\mu_f}\sqrt{A\Lambda}[f'' + 2\text{We}(f'')^2] \tag{18}$$

and

$$\text{Re}_x^{-\frac{1}{2}} Nu = -2\sqrt{\frac{A}{\Lambda}}\left[\frac{k_{\text{TCNF}}}{k_f} + 16R(1+\theta\theta_D) - 8R\right]\theta'(A), \tag{19}$$

where $\Lambda = r/x$ is the coordinate ratio parameter.

3. Results and Discussion

This section highlights physical interpretation of variation of flow velocity, fluid temperature, skin friction and Nusselt number subject to disparate physical parameters with their fixed values such as $\Omega = \pi/4$, $\lambda = 0.1$, $M = 1$, $L = 0.2$, $R = 0.1$, $\theta_D = 0.5$, Re $= 5$, Br $= 0.1$, Bi $= 1$, Pr $= 7.56$. The present explores the boundary layer flow and heat transfer of MWCNT + Al_2O_3 + TiO_2 + water TCNF subject to arbitrarily inclined (horizontal-inclined and vertical-inclined) thin needle under the influence of linear slip ($\delta = 0$) and nonlinear slip ($\delta \neq 0$) conditions.

3.1. *Representative profiles of fluid velocity*

On the onset of the discussion, let us come to Fig. 3 which indicates the variation of velocity $f'(\eta)$ of for sundry magnetic parameter M where rise in $M(M = 1, 1.5, 2)$ leads to controlled motion of TCNF under the influence of both linear and nonlinear slips for horizontal-inclined thin needle. In fact, rise in magnetic parameter intensifies the strength of Lorentz force which in turn impedes the fluid motion effectively. In case of horizontal-inclined, thin needle linear slip dominates over nonlinear unless until pressure difference is taken into consideration. This means that at fixed magnetic field strength $f'(\eta)$ attains higher value under the impact of linear slip than nonlinear slip. Velocity profiles in the form of overshoots appear in vicinity of thin needle surface for both types of slips. This is because the velocity of TCNF is greater in the vicinity of the needle surface than that of the ambient fluid. Further to say

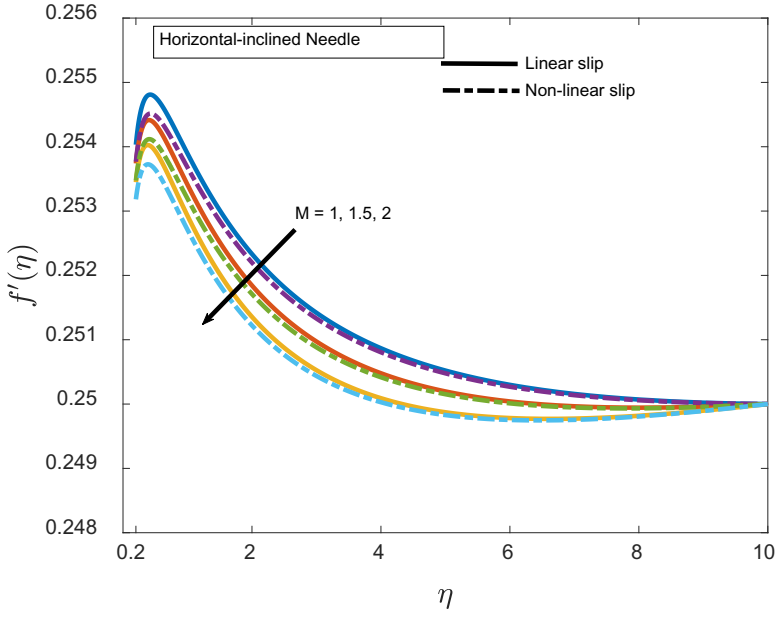

Fig. 3. (Color online) $f'(\eta)$ for different M and slips with horizontal-inclined needle.

that same decaying trend of $f'(\eta)$ appears for amplification of $M(M = 1, 1.5, 2)$ under the favor of both types of slips for fluid motion along vertical-inclined thin needle (Fig. 4). It is an amazing result that nonlinear slip dominates in respect of amelioration of $f'(\eta)$ than linear slip at particular strength of applied magnetic field.

3.2. *Representative profiles of fluid temperature*

Let us now explore the thermal behavior due to flow of TCNF over arbitrarily inclined (horizontal-inclined and vertical inclined) thin needle subject to linear and nonlinear slips under influence of pertinent parameters. Figure 5 reveals that rise in quadratic thermal radiation parameter $R(R = 0.1, 0.3, 0.5)$ leads to the upgradation of temperature distribution throughout the flow domain for both the slips. There is an amazing result that at low $R(R = 0.1)$, $\theta(\eta)$ attains greater magnitude in presence of nonlinear slip than linear slip. At moderate $R(R = 0.3)$, $\theta(\eta)$ attains greater value for linear slip than nonlinear one. However, at larger $R(R = 0.5)$ nonlinear slip dominates over linear slip in respect of intensification of $\theta(\eta)$ effectively. Increase in radiation parameter implicates more thermal radiation indicating more heat being received by the nearby TCNF from hot needle surface. As a result, the fluid temperature ameliorates. Figure 6 indicates that $\theta(\eta)$ ameliorates for rise in temperature difference parameter $\theta_D(\theta_D = 0.8, 1.5, 2)$ irrespective of nature of slips. In this case, the temperature of the TCNF near the surface of the hot thin needle is more than that of the ambient fluid. It is observed that linear slip dominates over nonlinear one

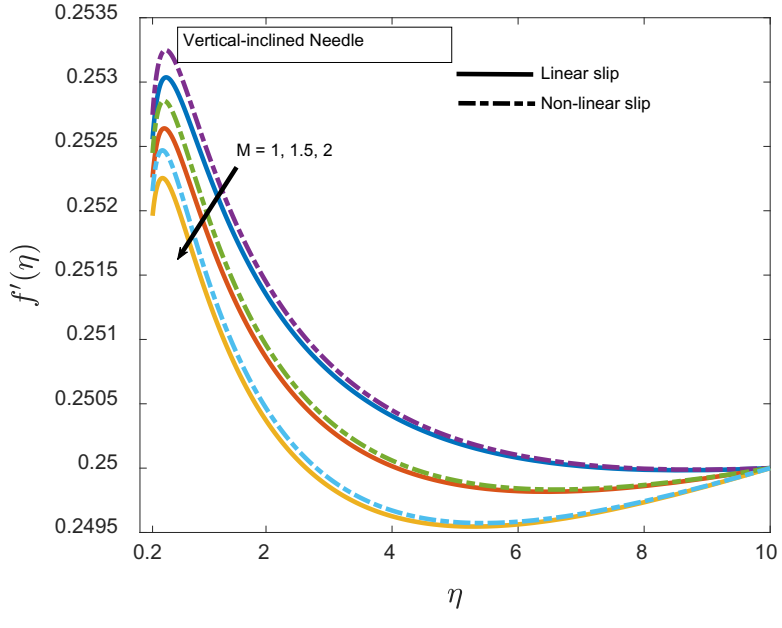

Fig. 4. (Color online) $f'(\eta)$ for different M and slips with vertical-inclined needle.

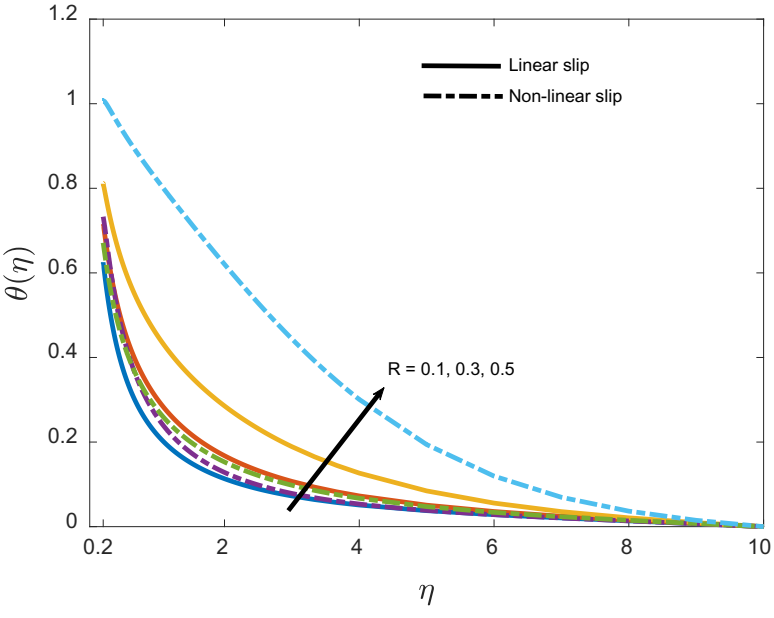

Fig. 5. (Color online) $\theta(\eta)$ for different R with linear and nonlinear slips.

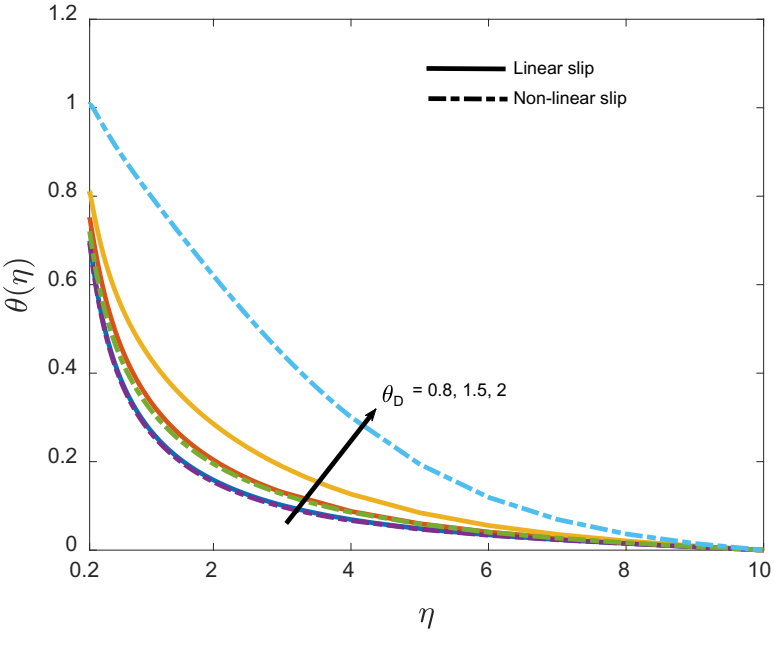

Fig. 6. (Color online) $\theta(\eta)$ for different θ_D with linear and nonlinear slips.

in enhancing $\theta(\eta)$ for low and moderate θ_D ($\theta_D = 0.8, 1.5$). However, opposite trend is visualized for higher θ_D ($\theta_D = 2$) exhibiting nonlinear slip dominance. Amplifying Reynolds number Re (Re $= 20, 40, 60$) yields diminution of $\theta(\eta)$ profiles in the entire boundary layer region. Physically, Reynolds number is the ratio of inertial force to viscous force. Increase in Reynolds number implicates more inertial force. This further accelerates the fluid motion effectively. Therefore, the nanoparticles stay less time in the flow region contiguous to the solid boundary. Consequently, the fluid temperature peters out. Lower value of Re (Re $= 20$) contributes the dominancy of linear slip, however, higher values of Re (Re $= 40, 60$) accounts for the dominancy of nonlinear slip in effective augmenting $\theta(\eta)$ distributions (Fig. 7). Further, Fig. 8 implicates that rise in Brinkman number Br (Br $= 0.2, 0.4$) upgrades $\theta(\eta)$ significantly. Physically, Brinkman number is the ratio of direct heat conduction from the needle surface to the viscous heat generated by shear in the boundary layer. Increase in Brinkman number leads to more heat produced by heat transport through molecular conduction thereby intensifies the fluid temperature. At low Br, $\theta(\eta)$ variation is insignificant, however, it is prominent at higher Br (exhibiting nonlinear slip dominancy). Rise in magnetic parameter M ($M = 1, 1.5, 2$) upsurges $\theta(\eta)$ for both the slips. Linear slip dominates in uplifting $\theta(\eta)$ in the domain of lower magnetic field strength; however, it reverses in the domain of higher magnetic field strength (Fig. 9).

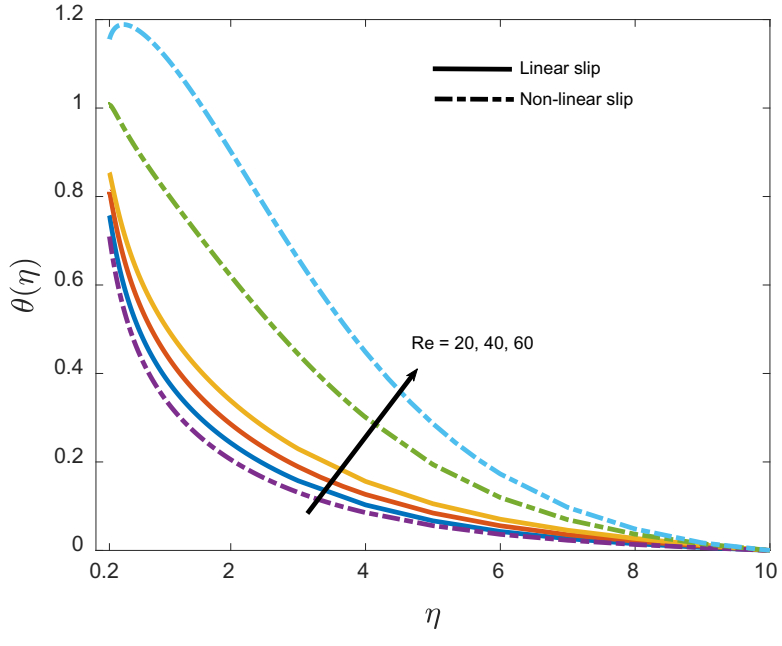

Fig. 7. (Color online) $\theta(\eta)$ for different Re with linear and nonlinear slips.

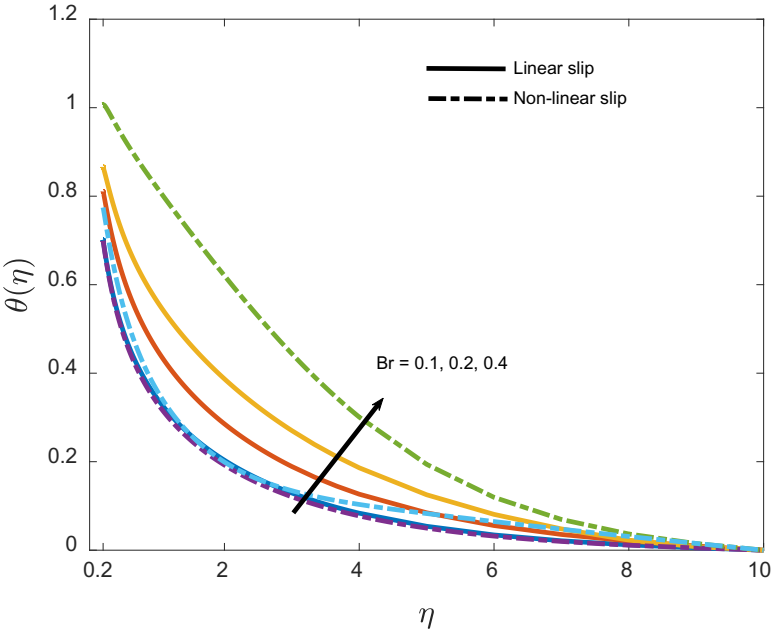

Fig. 8. (Color online) $\theta(\eta)$ for different Br with linear and nonlinear slips.

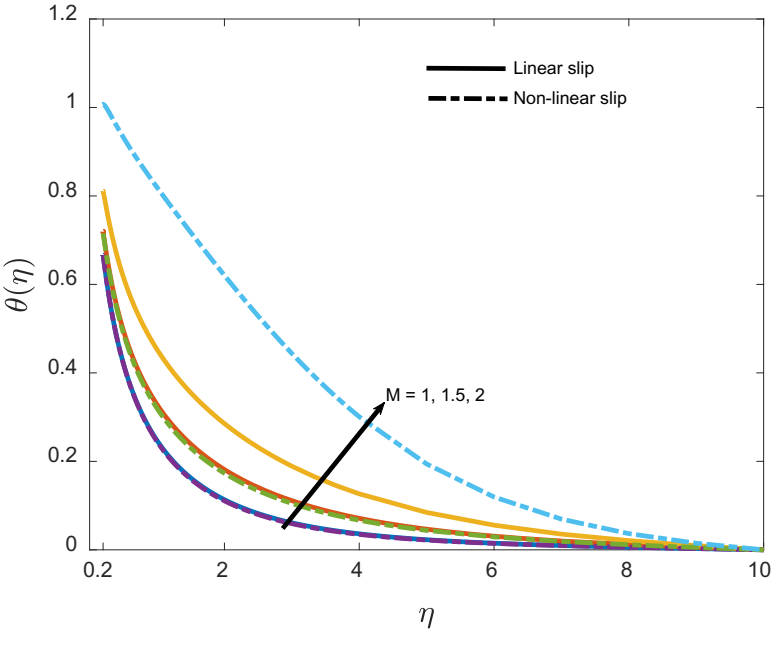

Fig. 9. (Color online) $\theta(\eta)$ for different M with linear and nonlinear slips.

It is obvious that increase in magnetic parameter enhances Lorentz force which offers resistance to the fluid motion. Therefore, nanoparticles experiences long duration near the hot needle surface. As a result, temperature of TCNF elevates. When Biot number Bi amplifies, $\theta(\eta)$ lifts up irrespective of type of slips (linear or nonlinear). Lower Bi (Bi $= 3$) yields the dominancy of linear slip, however, higher Bi (Bi $= 6, 10$) is responsible for the dominancy of nonlinear slip in the intensification of $\theta(\eta)$ distribution. The $\theta(\eta)$ amelioration is most prominent for high Bi(Bi $= 10$) influenced by nonlinear slip mechanism (Fig. 10). It is due to the fact that rise in Biot number indicates more convective heating by the hot fluid beneath the needle surface thereby enhancing the temperature of the TCNF within the boundary layer region.

3.3. *Representative profiles of skin friction and Nusselt number*

The variation of skin friction $\left(\mathrm{Re}_x^{\frac{1}{2}} C_f\right)$ for different values of size of thin needle A, M, L under the influence of linear and nonlinear slips is mentioned in Table 3. Rise in size of thin needle $(A = 0.1, 0.2, 0.3)$ accounts for the amelioration of skin friction (surface viscous drag) for both linear and nonlinear slips for moving horizontal-inclined needle. Further, rise in M, L yields emaciation of surface viscous drag for both slips for horizontal-inclined needle. Table 4 conveys surface viscous drag $\left(\mathrm{Re}_x^{\frac{1}{2}} C_f\right)$ variation in response to disparate pertinent parameters A, M, L subject to both linear and nonlinear slips for a vertical-inclined thin needle. It is obtained that

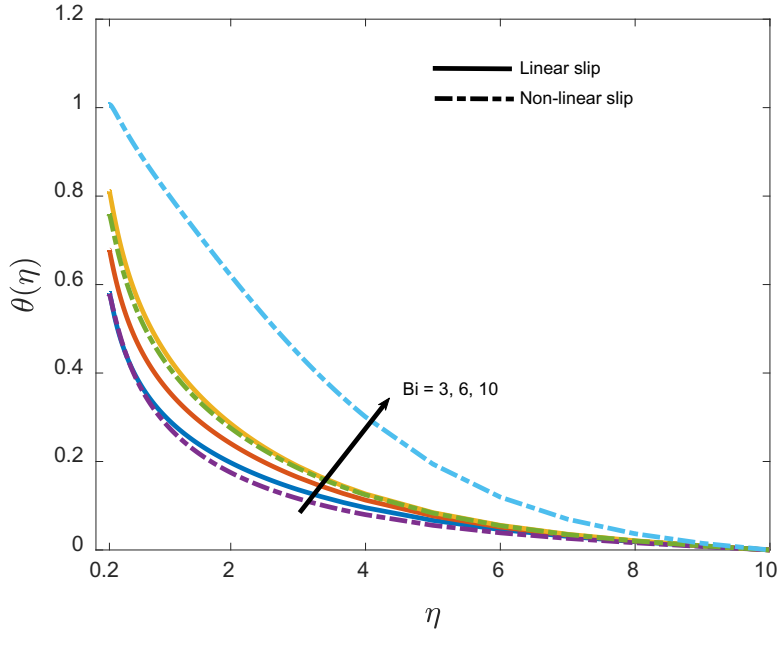

Fig. 10. (Color online) $\theta(\eta)$ for different Bi with linear and nonlinear slips.

Table 3. Skin friction for horizontal-inclined needle with linear and nonlinear slips.

			$\mathrm{Re}_x^{\frac{1}{2}} C_f$	
A	M	γ	Linear slip ($\delta = 0$)	Nonlinear slip ($\delta \neq 0$)
0.1	1	0.2	0.00811	0.00859
0.2			0.01165	0.01249
0.3			0.01337	0.01442
0.2	1.5		0.01070	0.01156
	2		0.00978	0.01062
		0.1	0.01443	0.01549
		0.3	0.00975	0.01047
			0.01186	0.01273
			0.01207	0.01299

Table 4. Skin friction for vertical-inclined needle with linear and nonlinear slips.

			$\mathrm{Re}_x^{\frac{1}{2}} C_f$	
A	M	γ	Linear slip ($\delta = 0$)	Nonlinear slip ($\delta \neq 0$)
0.2	1	0.2	0.00780	0.00839
0.1			0.00530	0.00565
0.3			0.00902	0.00978
0.2	1.5		0.00687	0.007467
	2		0.00594	0.00655
		0.1	0.00967	0.01040
		0.3	0.00653	0.00703
			0.00789	0.00851
			0.00799	0.00862

rise in A upgrades $\mathrm{Re}_x^{\frac{1}{2}} C_f$ while that of M and L declines it for both slips for the flow of TCNF due to vertical-inclined thin needle. Table 5 informs the variation of Nusselt number $\left(\mathrm{Re}_x^{-\frac{1}{2}}\mathrm{Nu}\right)$ for disparate $R, \theta_D, \mathrm{Re}, \mathrm{Br}$ for both linear and nonlinear slips inducing the flow of TCNF along vertical-inclined thin needle tilting at an angle $\Omega = \pi/4$. It is visualized that rise in size of the needle A and Bi ameliorates the heat transfer rate from the surface of thin needle while that of $R, \theta_D, \mathrm{Re}, \mathrm{Br}, M$ follows decreasing trend.

3.4. *Validation*

We have compared our results with the existing literature of Soid *et al.*[39] and Madhukesh *et al.*[40] for $f''(A)$ with horizontal needle under certain constraints which shown in Table 6 and we have observed a very good agreement with those results. It gives us confidence in our numerical scheme and outcomes.

Table 5. Nusselt number for linear and nonlinear slips with $\Omega = \pi/4$.

							$\mathrm{Re}_x^{-\frac{1}{2}}\mathrm{Nu}$	
R	θ_D	Re	Br	M	Bi	A	Linear slip ($\delta = 0$)	Nonlinear slip ($\delta \neq 0$)
0.5	2	40	0.2	2	10	0.2	7.46678	7.29223
0.1							6.76817	6.72427
0.3							6.57192	5.29463
	0.8						8.05564	7.94101
	1.5						7.44219	6.86482
		20					9.59265	9.25129
		60					5.74365	4.81961
			0.1				9.37406	9.23124
			0.4				8.06025	8.02903
				1			11.11404	11.00727
				1.5			9.91003	9.60001
					3		4.04129	4.00967
					6		7.24794	5.93737
							6.24869	5.41247
							4.38542	3.39957
						0.1	3.25253	3.42693
						0.3	8.57119	8.83728

Table 6. Validation with the existing literature for $f''(A)$ with horizontal needle and $\phi_1 = \phi_2 = \mathrm{We} = \lambda_1 = M = R = \mathrm{Br} = \gamma = 0$, $\mathrm{Bi} \to \infty$ when $\mathrm{Pr} = 6.2$ and $A = 0.1$.

	Soid *et al.*[39]	Madhukesh *et al.*[40]	Present
$\varepsilon = 0$	1.288778	1.289731	1.2889732
$\varepsilon = -1$	3.703713	3.711607	3.7091349

4. Conclusions

Flow and heat transfer aspects of TCNF (MWCNT + Al_2O_3 + TiO_2 + water) induced by linear and nonlinear slips over arbitrarily inclined moving thin needle are investigated in this study. Because of synergistic effect of TCNFs, they possess better thermophysical and rheology properties thereby acting as better suitable heat transfer fluid in wire coating, metal spinning, aerodynamics, transportation, lubrication medicine, engineering industries, etc., subject to flow and heat transfer over thin needle. Modified Thompson and Troian nonlinear slip and quadratic thermal radiation phenomena are newly introduced in this study. Fourth-order Runge–Kutta method is implemented to obtain requisite numerical solution. The major outcomes of the present investigation are highlighted as follows:

- It is accomplished that $f'(\eta)$ peters out with amplification of M due the flow of TCNF, MWCNT + Al_2O_3 + TiO_2 + water induced by either linear slip or nonlinear slip.

- Lower value of Re, Bi favors the dominancy of linear slip, however, higher values of Re, Bi account for the dominancy of nonlinear slip in effective intensification of $\theta(\eta)$ distributions.
- Surface viscous drag intensifies due to rise in A while that exhibits reverse nature with increment in M for both slips inducing the flow of TCNF over thin needle irrespective of its positions.
- It is remarked that rise in size of thin needle and convective heating ameliorates heat transfer rate from the surface of inclined ($\Omega = \pi/4$) moving thin needle due to the flow of TCNF induced by both linear and nonlinear slips.

References

1. S. K. Das *et al.*, *Nanofluids: Science and Technology* (John Wiley and Sons, 2007).
2. M. Sheikholeslami, M. M. Rashidi and D. D. Ganji, *J. Mol. Liq.* **212**, 117 (2015).
3. S. U. S. Choi, Enhancing thermal conductivity of fluids with nanoparticles, Developments and Applications of Non-Newtonian Flows (American Society of Mechanical Engineers, 1995), pp. 99–105.
4. A. K. Hakeem, M. K. Nayak and O. D. Makinde, *J. Appl. Comput. Mech.* **5**, 390 (2019), doi: 10.22055/JACM.2018.26307.1322.
5. A. T. Akinshilo, *Bionanoscience* **9**, 740 (2019).
6. M. K. Nayak, G. C. Dash and L. P. Singh, *J. Appl. Anal. Comput.* **4**, 367 (2014).
7. G. M. Sobamowo and A. T. Akinshilo, *Appl. Comput. Mech.* **11**, (2017), doi: 10.24132/acm.2017.367.
8. M. K. Nayak *et al.*, *J. Taiwan Inst. Chem. Eng.* **128**, 288 (2021).
9. A. T. Akinshilo and H. Ali, *J. Appl. Comput. Mech.* **6**, 433 (2020).
10. M. K. Nayak *et al.*, *Propul. Power Res.* **8**, 339 (2019).
11. A. T. Akinshilo, *Phys. Scr.* **95**, 125702 (2020).
12. A. M. Zidan *et al.*, *J. Build. Eng.* **53**, 104550 (2022).
13. G. M. Sobamowo and A. T. Akinshilo, *Alexandria Eng. J.* **57**, 1413 (2018).
14. M. K. Nayak *et al.*, *Sustain. Energy Technol. Assess.* **52**, 102180 (2022).
15. A. T. Akinshilo and A. O. llegbusi, *J. Therm. Eng.* **5**, 482 (2019).
16. S. S. Chougule and S. K. Sahu, Model of heat conduction in hybrid nanofluid, in *2013 IEEE Int. Conf. Emerging Trends in Computing, Communication and Nanotechnology (ICECCN)* (IEEE, 2013), pp. 337–341.
17. A. T. Akinshilo, F. Mabood and I. A. Badruddin, *Waves Random Complex Media* 1 (2022), doi: 10.1080/17455030.2022.2117432.
18. X. Wang, X. Xu and S. U. Choi, *J. Thermophys. Heat Transf.* **13**, 474 (1999).
19. P. Selvakumar and S. Suresh, *IEEE Trans. Compon. Packag. Manuf. Technol.* **2**, 1600 (2012).
20. D. Huang, Z. Wu and B. Sunden, *Exp. Therm. Fluid Sci.* **72**, 190 (2016).
21. M. K. Nayak *et al.*, *Waves. Random Complex Media* **32**, 1 (2020), doi: 10.1080/17455030.2022.2032474.
22. M. K. Nayak *et al.*, *Int. J. Numer. Methods Heat Fluid Flow* **32**, 1861 (2022).
23. A. Dezfulizadeh *et al.*, *Powder Technol.* **389**, 215 (2021).
24. Z. Xuan *et al.*, *J. Mol. Liq.* **323**, 114889 (2021), doi: 10.1016/j.molliq.2020.114889.
25. R. R. Sahoo, *Powder Technol.* **370**, 19 (2020).
26. F. Quero and A. Rosenkranz, *Adv. Mater. Interfaces* **8**, 2100952 (2021), doi: 10.1002/admi.202100952.
27. A. Boroomandpour, D. Toghraie and M. Hashemian, *Synth. Met.* **268**, 116501 (2020).

28. S. Kashyap, J. Sarkar and A. Kumar, *Energy* **225**, 120199 (2021).
29. M. K. Sarangi *et al.*, *Int. Commun. Heat Mass Transf.* **138**, 106337 (2022).
30. M. K. Sarangi *et al.*, *Mater. Sci. Eng. B* **287**, 116124 (2023).
31. L. L. Lee, *Phys. Fluids* **10**, 1820 (1967).
32. A. Ishak, R. Nazar and I. Pop, *Chin. Phys. Lett.* **24**, 2895 (2007).
33. S. Ahmad *et al.*, *Int. Commun. Heat Mass Transf.* **35**, 157 (2008).
34. M. W. A. Khan *et al.*, *Physica B* **534**, 113 (2018).
35. A. T. Akinshilo, F. Mabood and A. O. llegbusi, *Int. Commun. Heat Mass Transf.* **127**, 105547 (2021).
36. M. K. Nayak, F. Mabood and O. D. Makinde, *Heat Transf.* **49**, 655 (2020).
37. F. Mabood *et al.*, *Phys. Scr.* **95**, 115219 (2020).
38. H. Adun *et al.*, *J. Energy Storage* **51**, 104531 (2022).
39. S. K. Soid, A. Ishak and I. Pop, *Appl. Therm. Eng.* **114**, 58 (2017), doi: 10.1016/j.applthermaleng.2016.11.165.
40. J. K. Madhukesh *et al.*, *Waves Random Complex Media* 1 (2021), doi: 10.1080/17455030.2021.2012303.